THE JOURNAL OF PHYSICAL CHEMISTRY C

pubs.acs.org/JPCC Article

Elucidation of Photocatalytic Properties of Gold–Platinum Bimetallic Nanoplates Using Tip-Enhanced Raman Spectroscopy

Zhandong Li and Dmitry Kurouski*

Cite This: https://dx.doi.org/10.1021/acs.jpcc.0c04274 Read Online

ACCESS | Metrics & More | Article Recommendations | Supporting Information

ABSTRACT: Plasmonic catalysis is based on a unique property of noble metal nanostructures to harvest electromagnetic radiation converting it into hot carriers. These high energy species can catalyze chemical reactions in molecules located in the vicinity to surfaces of the plasmonic nanostructures. However, traditional plasmonic metals such as gold (Au) are useful only for a limited number of chemical reactions. The spectrum of chemical reactions can be broadened up by coupling plasmonic and catalytic metals, such as platinum (Pt), in one nanostructure. In this study, we use tip-enhanced Raman spectroscopy (TERS) to probe photocatalytic properties of gold–platinum nanoplates (Au@PtNPs). We found that Au@PtNPs highly efficiently proto-reduced 4-nitrobenzenethiol (4-NBT) to *p*,*p*′-dimercaptoazobisbenzene (DMAB) with the yield similar to the one observed for gold nanoplates (AuNPs). These Au@PtNPs could be used to proto-oxidize 4-aminothiophenol (4-ATP) first to 4-NBT and then 4-NBT to DMAB, whereas photo-oxidation of 4-ATP on the surface of AuNPs directly proceeds to DMAB.

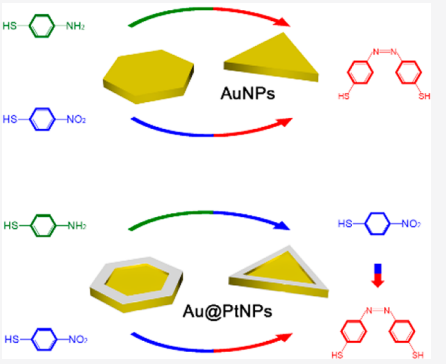

Illumination of noble metal nanostructures by electromagnetic radiation induces collective oscillations of electrons at the surface of nanostructures.[1−6] These collective oscillations of electrons or localized surface plasmon resonances (LSPRs) are the underlying cause of surface-enhanced Raman scattering (SERS) phenomenon.[7−10] LSPRs can decay forming hot carriers through direct interband, phonon-assisted intraband, and geometry-assisted transitions.[11−13] These hot carriers are highly energetic species that persist over a few tens of femtoseconds to picoseconds time scale.[14,15] Hot carriers can further decay via electron−electron or electron−phonon scattering or can populate unoccupied orbitals in molecules located at the close vicinity to metal surfaces.[16,17] In the latter scenario, hot carriers can catalyze chemical reactions, such as O_2 and H_2 dissociation,[18,19] photo-oxidation of 4-aminothiophenol (4-ATP), and photoreduction of 4-nitrobenzenethiol (4-NBT) to *p*,*p*′-dimercaptoazobisbenzene (DMAB).[20,21] Although noble metal nanostructures exhibit high efficiency of such catalytic reactions, their selectivity is limited.

This problem can be overcome by the coupling of noble metals with catalytic metals such as palladium (Pd), ruthenium (Ru), or platinum (Pt) in a bimetallic construct. Such bimetallic nanostructures exhibit a broad spectrum of catalytic reactions and higher reaction rates relative to their monometallic counterparts.[22,23] For instance, Wang and co-workers showed that Au@Pd nanostructures demonstrated 2-fold enhancement of rates of Suzuki coupling in comparison to rates of reactions thermally heated to the same temperature.[24] The researchers also reported a 2-fold increase in the reaction yield provided by these Au@Pd nanostructures relative to the rates of their monometallic counterparts. At the same time, there is very little known about nanoscale catalytic properties of such bimetallic nanostructures as well the selectivity of photocatalytic reactions that are performed by them.

Tip-enhanced Raman spectroscopy (TERS) is a modern analytical technique that provides detailed chemical information single-molecule sensitivity.[25−27] Specially, TERS provides high spatial resolution allowing for monitoring chemical reactions in real-time,[25,26] which may not be possible using SERS. This makes TERS perfectly suitable for elucidation of selectivity of photocatalytic processes on both mono- and bimetallic nanostructures.[28−30] Recently, our group showed that TERS can be used to probe catalytic efficiency of 4-NBT to DMAB conversion of different crystal phases of Au microplates (AuMPs).[31] It has been found that Au (111) has much higher catalytic activity comparing to Au (110) and Au (100) facets. It has been also found that in addition to DMAB, 4-NBT can be converted to 4-nitrobenzenethiolate.[32]

In this study, we used TERS to investigate reaction products of photo-oxidation of 4-ATP and photoreduction of 4-NBT on the surface of gold–platinum nanoplates (Au@PNPs). Our findings show that Au@PtNPs proto-reduce 4-NBT to DMAB

Received: May 12, 2020
Published: May 15, 2020

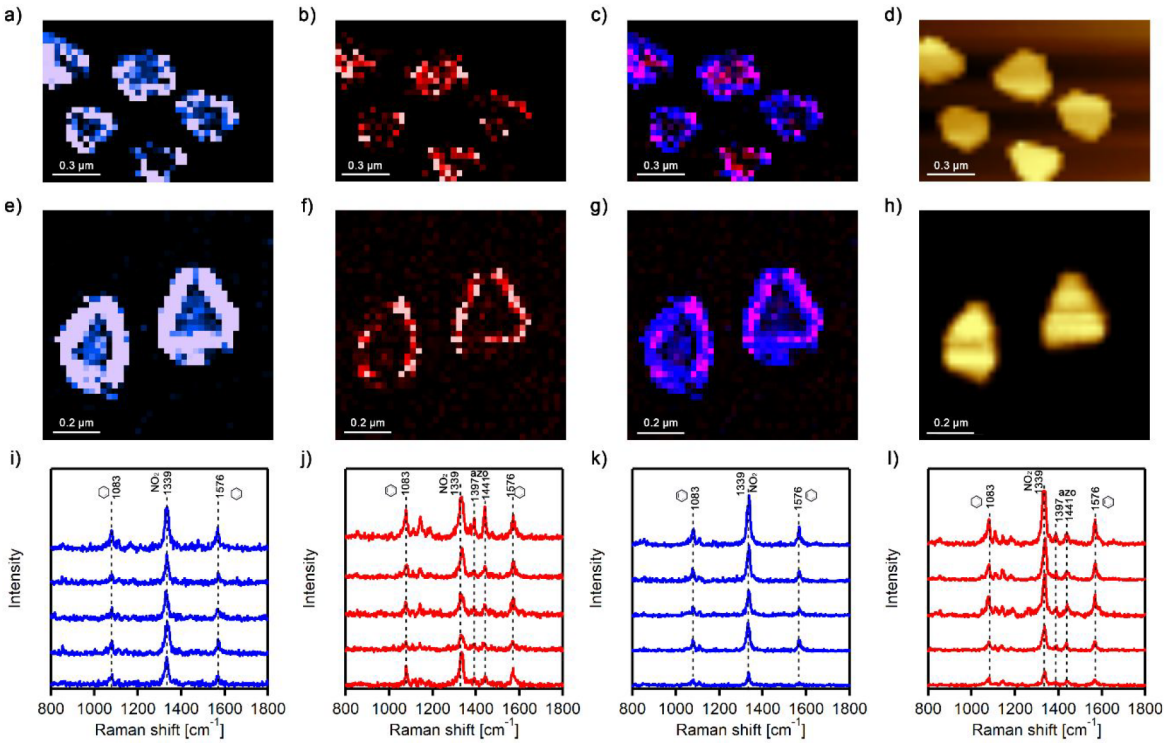

Figure 1. Photo reduction of 4-NBT to DMAB on AuNPs and Au@PtNPs. (a) TERS image of Au@PtNPs with a monolayer of 4-NBT (intensity of 1339 cm^{-1} band (NO_2 vibration) of 4-NBT is shown in blue); (b) TERS image of DMAB on Au@PtNPs (intensity of 1395 and 1448 cm^{-1} bands (N = N vibration) of DMAB is shown in red); (c) TERS image of Au@PtNPs with both NO_2 and N = N vibrations; (d) corresponding AFM image of Au@PtNPs.; (e) TERS image of AuNPs with a monolayer of 4-NBT; (f) TERS image of DMAB on AuNPs of DMAB; (g) TERS image of AuNPs with both NO_2 and N = N vibrations; (h) corresponding AFM image of AuNPs. Typical TERS spectra of 4-NBT (i) and DMAB (j) on Au@PtNPs and 4-NBT (k) and DMAB (l) on AuNPs. The TERS spectra are randomly chosen from the corresponding TERS map with the same laser power and acquisition time at each point. The resolution in each of TERS image is 20 nm per pixel.

with the yield similar to the one observed for AuNPs. However, Au@PtNPs proto-oxidize 4-ATP first to 4-NBT and then 4-NBT to DMAB, whereas AuNPs instantly carry such oxidation directly to DMAB. These findings suggest that Au@PtNPs have higher reaction selectivity relative to their monometallic analogs.

Au@PtNPs and AuNPs used in this study were ∼200 nm trigonal/hexagonal nanostructures with 60−70 nm in thicknesses, Figure 1d, Figure S1, and Figure S2. A monolater of 4-nitrobenzenethiol (4-NBT) was deposited on the surfaces of both Au@PtNPs and AuNPs and used as a molecule reporter in the TERS experiments. TERS measurements were conducted on AIST-NT-HORIBA system equipped with a 633 nm CW laser. The laser was brought to the sample in a side-illumination (45° angle) geometry; laser power used throughout the TERS experiments was approximately 30 μW. TERS probes were fabricated through metal deposition of 70 nm of Au on the Si tip (Appnano (Mountain View, CA), 1 kHz scanning frequency). The tip-fabrication procedure is described in detail in the Supporting Information. TERS spectrum of 4-NBT has three distinct vibrational bands as fingerprint at 1083, 1339, and 1576 cm^{-1} (Figure 1i). We found that on the surface of Au@PtNPs, 4-NBT could be photochemically reduced to p,p'-dimercaptoazobisbenzene (DMAB), which features a doublet of peaks at 1397 and 1441 cm^{-1} (Figure 1j). Nanoscale TER imaging of Au@PtNPs (Figure 1a,b) revealed random spots of DMAB formation observed at both the edges and terraces of the bimetallic nanostructures (Figure 1c).

One may wonder whether analogous photocatalytic conversion could be achieved on AuNPs. To answer this question, we used TERS to image the surface of monometallic AuNPs with a monolayer of 4-NBT (Figure 1e). AuNPs had similar dimensions to Au@PtNPs: ∼200 nm in length with thicknesses of 60−70 nm. We have found that on the surface of AuNPs, 4-NBT could be also catalyzed to DMAB (Figure 1f,l); however, the photoreduction took place primarily along edges of the AuNPs (Figure 1f,g). This high photocatalytic efficiency of edges can be explained by localization of electric field and excitation of plasmon modes along the edges and corners of noble metal nanostructures.[33] In contrast, such edge effect is absent on Au@PtNPs, which suggests more even distribution of electric field in these bimetallic nanostructures.[22,23]

Noble metal nanostructures have both proto-reduction and photo-oxidation properties. Tian group reported that 4-ATP can be photocatalytically oxidized to DMAB by Au nanoparticles (AuNPs).[20,21] Following on this discovery, we used TERS to investigate nanoscale photo-oxidation properties of both Au@PtNPs and AuNPs with monolater of 4-ATP on their surface (Figure 2). Raman spectrum of 4-ATP showed the NH_2 band at 1591 cm^{-1} (Figure 2i,k), which agrees well with the previously reported spectra of this molecule.[20,21] We found that 4-ATP become spontaneously oxidized to DMAB on the surface of AuNP (Figure 2b,c). Similar to 4-NBT reduction, the sides and corners of AuNPs exhibited the strongest activity of 4-ATP to DMAB photo-oxidation. However, we found that the photo-oxidation of 4-ATP on the surface of Au@PtNPs did not result in DMAB formation.

https://dx.doi.org/10.1021/acs.jpcc.0c04274
J. Phys. Chem. C XXXX, XXX, XXX−XXX

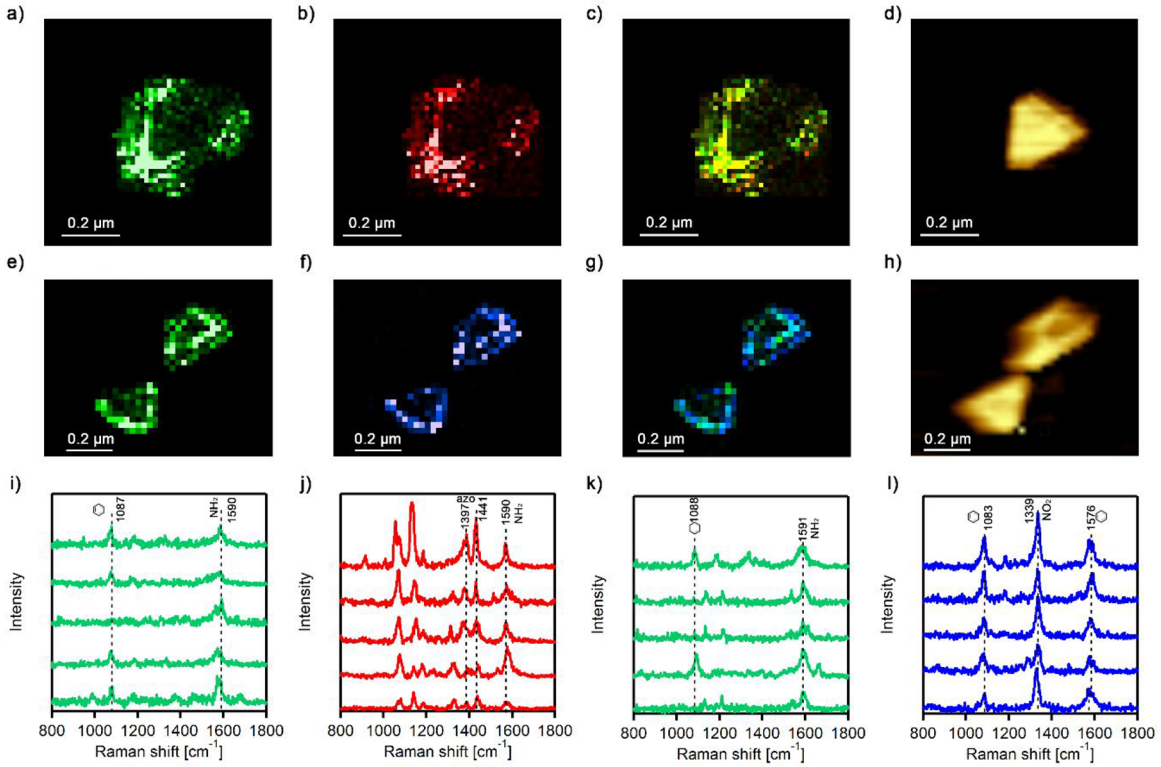

Figure 2. Photo oxidation of 4-ATP to DMAB and 4-NBT. (a) TERS image of 4-ATP and (b) DMAB, as well as (c) TERS image of AuNPs with both NO_2 and N = N vibrations; (d) corresponding AFM image of AuNPs; (e) TERS image of 4-ATP on Au@PtNPs; (f) TERS image of 4-NBT on Au@PtNPs; (g) TERS image of Au@PtNPs from the overlapping of NH_2 and NO_2 vibrations. Intensity of 1590 cm^{-1} band (NH_2 vibration) of 4-ATP is shown in green, intensity of 1339 cm^{-1} band (NO_2 vibration) of 4-NBT is shown in blue, intensity of 1397, 1441 cm^{-1} band (azo vibration) of DMAB is shown in red. (h) CorrespondingAFM image of Au@Pt NPs; (i–j) Typical TERS spectra extracted from chemical maps on AuNPs (parts a–c) showing presence of 4-ATP (green), DMAB (red). (k–l) Typical TERS spectra extracted from chemical maps on AuNPs (parts e–g) showing presence of 4-ATP (green), and 4-NBT (blue). The resolution in each of TERS image is 20 nm per pixel with 0.5 s acquisition time.

Instead, we observed 4-ATP to 4-NBT conversion, Figure 2e–h). Nanoscale imaging of the active sites of 4-ATP photo-oxidation revealed that similar to AuNPs, this process was taking place at the edges and tips of these bimetallic nanostructures. Thus, edges and corners of Au@PtNPs are more active in photo-oxidation, whereas the whole surface of these nanostructures has nearly equal activity in photo-reduction (4-NBT to DMAB reduction).

This result was rather surprising because Au@PtNPs could oxidize 4-NBT to DMAB, as was discussed above. We found that an increase of the tip exposure time on the surface of Au@PtNPs resulted in the photo-oxidation of 4-NBT to DMAB, Figure 3. By other means, more energy is required to photoconvert 4-ATP to DMAB on the surface of Au@PtNPs in comparison to that of their monometallic analogs (AuNPs). TERS imaging also revealed that 4-NBT molecules located on the perimeter of Au@PtNPs were photo-oxidized into DMAB, as well as some 4-ATP located on the terraces of these bimetallic nanostructures. These findings can be explained by LSPRs damping in such bimetallic nanostructures due to increased probability of interband transitions.[34,35] The last can be attributed to close energy levels of d-bands and Fermi levels in Pt (Figure S3). Such LSPRs damping has been previously reported for Au@Pd nanorods and Au@Pt nanoparticles.[34,36] At the same time, no LSPR damping is taking place on monometallic nanostructures (AuNPs), which explains their so-called gap-mode enhancement effect in TERS. These findings also suggest that a higher intensity of electric field is required to enable the photo-oxidation of 4-ATP to DMAB relative to the intensity of the electric field necessary for the photoreduction of 4-NBT to DMAB, Figure 4.

This hypothesis is supported by the experimental evidence reported by Wang and co-workers.[37] The researchers have shown that such selectivity of 4-ATP photo-oxidation could be achieved via presence of titanium oxide (TiO_2) nanoparticles on the surface of AuNPs (TiO_2–AuNPs). It was found that under UV illumination, TiO_2–AuNPs photo-oxidize 4-ATP to 4-NBT. If UV illumination was removed, 4-NBT molecules that were present on the surface of TiO_2–AuNPs appeared to be spontaneously further photo-oxidized to DMAB. At the same time, such selectivity could not be achieved for 4-NBT to DMAB formation which was occurring instantaneously on the surface of both TiO_2–AuNPs and their monometallic analogs (AuNPs). Wang and coauthors proposed that UV-driven selectivity of TiO_2–AuNPs could be explained by hot-electron pairing with holes in TiO_2. We expect that the underlying physical principles that determine catalytic selectivity obe-served on TiO2-AuNPs and Au@PtNPs are different. Additional experiments are required for a direct comparison of these catalytic systems upon identical environmental/experimental conditions, which is beyond the scope of current work.

Using TERS, we have systematically investigated photo-catalytic properties of both bi- and monometallic nanostruc-

https://dx.doi.org/10.1021/acs.jpcc.0c04274
J. Phys. Chem. C XXXX, XXX, XXX–XXX

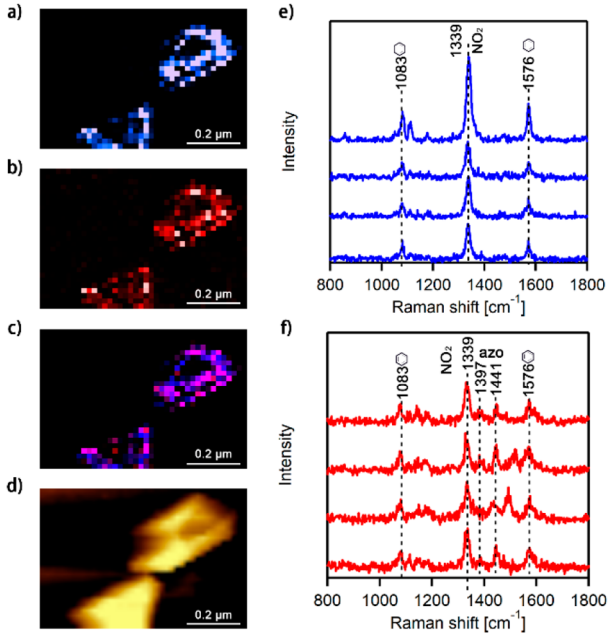

Figure 3. Second round TERS after oxidation of 4-ATP to 4-NBT. (a) TERS image of 4-NBT on Au@Pt NPs. Intensity of 1339 cm^{-1} band (NO_2 vibration) of 4-NBT is shown in blue. (b) TERS image of DMAB on Au@Pt NPs. Intensity of 1397 and 1441 cm^{-1} band (azo vibration) of DMAB is shown in red. (c) TERS image of Au@Pt NPs from the overlapping of NO_2 and azo vibrations. (d) Corresponding AFM image of Au@Pt NPs; (e, f) Typical TERS spectra extracted from chemical maps on Au@Pt NPs (parts a, b, and c) showing presence of 4-NBT (blue), 4-DMAB (red). The resolution in each of TERS image is 20 nm per pixel with 1 s acquisition time.

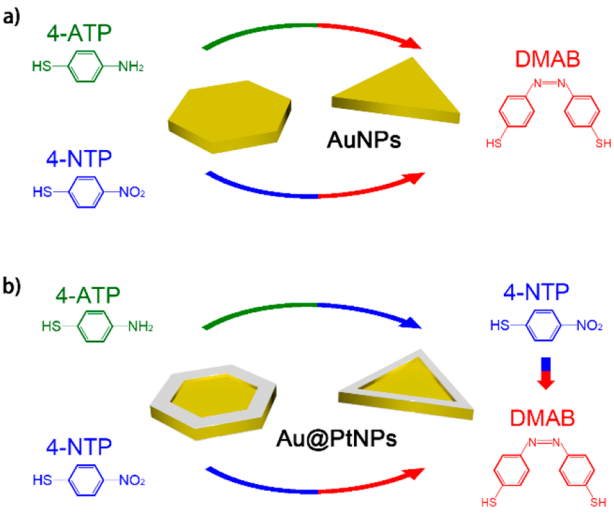

Figure 4. Photo catalyzation route of 4-ATP and 4-NBT on (a) AuNPs and (b) Au@PtNPs.

tures. Our results demonstrate that both Au@PtNPs and AuNPs can photoreduce 4-NBT to DMAB. However, they perform the photo-oxidation of 4-ATP with unequal efficiency. This reaction spontaneously occurs on the surface of AuNPs, whereas on Au@PtNPs, 4-ATP is first photo-oxidized to 4-NBT and only afterward to DMAB. This can be explained by LSPR damping in the interband transitions of Pt. These findings suggest that a stronger electric field is required to perform photo-oxidation reactions on Au@PtNPs relative to AuNPs. One can expect that the efficiency and selectivity of such photo-oxidation processes are strongly correlated with the metal composition of these nanostructures. We expect that our finding will inspire the rational design of new generation of mono/bimetallic nanomaterials toward controllable, selective, and highly efficient catalysis.

■ ASSOCIATED CONTENT

Supporting Information

The Supporting Information is available free of charge at https://pubs.acs.org/doi/10.1021/acs.jpcc.0c04274.

Detailed experimental procedure and AFM images of reported AuNPs and Au@PtNPs (PDF)

■ AUTHOR INFORMATION

Corresponding Author

Dmitry Kurouski − *Department of Biochemistry and Biophysics and The Institute for Quantum Science and Engineering, Texas A&M University, College Station, Texas 77843, United States;* orcid.org/0000-0002-6040-4213; Email: dkurouski@tamu.edu

Author

Zhandong Li − *Department of Biochemistry and Biophysics, Texas A&M University, College Station, Texas 77843, United States*

Complete contact information is available at: https://pubs.acs.org/10.1021/acs.jpcc.0c04274

Notes

The authors declare no competing financial interest.

■ ACKNOWLEDGMENTS

We are grateful to AgriLife Research of Texas A&M for the provided financial support. We also acknowledge Governor's University Research Initiative (GURI) grant program of Texas A&M University, GURI Grant Agreement No. 12-2016, M1700437.

■ REFERENCES

(1) Kleinman, S. L.; Frontiera, R. R.; Henry, A. I.; Dieringer, J. A.; Van Duyne, R. P. Creating, characterizing, and controlling chemistry with SERS hot spots. *Phys. Chem. Chem. Phys.* **2013**, *15*, 21−36.

(2) Brown, R. J.; Milton, M. J. T. Nanostructures and nanostructured substrates for surface-enhanced Raman scattering (SERS). *J. Raman Spectrosc.* **2008**, *39*, 1313−1326.

(3) Moskovits, M. Surface roughness and the enhanced intensity of Raman scattering by molecules adsorbed on metals. *J. Chem. Phys.* **1978**, *69*, 4159−4161.

(4) Gersten, J.; Nitzan, A. Electromagnetic Theory of Enhanced Raman-Scattering by Molecules Adsorbed on Rough Surfaces. *J. Chem. Phys.* **1980**, *73*, 3023−3037.

(5) Kerker, M.; Wang, D. S.; Chew, H. Surface enhanced Raman scattering (SERS) by molecules adsorbed at spherical particles. *Appl. Opt.* **1980**, *19*, 3373−88.

(6) King, F. W.; Van Duyne, R. P.; Schatz, G. C. Theory of Raman scattering by molecules adsorbed on electrode surfaces. *J. Chem. Phys.* **1978**, *69*, 4472−4481.

(7) Kelly, K. L.; Coronado, E.; Zhao, L. L.; Schatz, G. C. The Optical Properties of Metal Nanoparticles: The Influence of Size, Shape, and Dielectric Environment. *J. Phys. Chem. B* **2003**, *107*, 668−677.

(8) Wustholz, K. L.; Henry, A. I.; McMahon, J. M.; Freeman, R. G.; Valley, N.; Piotti, M. E.; Natan, M. J.; Schatz, G. C.; Van Duyne, R. P.

Structure-activity relationships in gold nanoparticle dimers and trimers for surface-enhanced Raman spectroscopy. *J. Am. Chem. Soc.* **2010**, *132*, 10903−10.
(9) Haes, A. J.; Haynes, C. L.; McFarland, A. D.; Schatz, G. C.; Van Duyne, R. P.; Zou, S. Plasmonic Materials for Surface-Enhanced Sensing and Spectroscopy. *MRS Bull.* **2005**, *30*, 368−375.
(10) Ringe, E.; McMahon, J. M.; Sohn, K.; Cobley, C.; Xia, Y.; Huang, J.; Schatz, G. C.; Marks, L. D.; Van Duyne, R. P. Unraveling the Effects of Size, Composition, and Substrate on the Localized Surface Plasmon Resonance Frequencies of Gold and Silver Nanocubes: A Systematic Single-Particle Approach. *J. Phys. Chem. C* **2010**, *114*, 12511−12516.
(11) Khurgin, J. B. How to deal with the loss in plasmonics and metamaterials. *Nat. Nanotechnol.* **2015**, *10*, 2−6.
(12) Narang, P.; Sundararaman, R.; Atwater, H. A. Plasmonic hot carrier dynamics in solid-state and chemical systems for energy conversion. *Nanophotonics* **2016**, *5*, 96−111.
(13) Manjavacas, A.; Liu, J. G.; Kulkarni, V.; Nordlander, P. Plasmon-induced hot carriers in metallic nanoparticles. *ACS Nano* **2014**, *8*, 7630−7638.
(14) Brown, A. M.; Sundararaman, R.; Narang, P.; Goddard, W. A., III; Atwater, H. A. Nonradiative plasmon decay and hot carrier dynamics: effects of phonons, surfaces, and geometry. *ACS Nano* **2016**, *10*, 957−966.
(15) Hartland, G. V. Optical studies of dynamics in noble metal nanostructures. *Chem. Rev.* **2011**, *111*, 3858−3887.
(16) Ma, J.; Wang, Z.; Wang, L.-W. Interplay between plasmon and single-particle excitations in a metal nanocluster. *Nat. Commun.* **2015**, *6*, 1−11.
(17) Cortés, E.; Xie, W.; Cambiasso, J.; Jermyn, A. S.; Sundararaman, R.; Narang, P.; Schlücker, S.; Maier, S. A. Plasmonic hot electron transport drives nano-localized chemistry. *Nat. Commun.* **2017**, *8*, 1−10.
(18) Mukherjee, S.; Zhou, L.; Goodman, A. M.; Large, N.; Ayala-Orozco, C.; Zhang, Y.; Nordlander, P.; Halas, N. J. Hot-electron-induced dissociation of H2 on gold nanoparticles supported on SiO2. *J. Am. Chem. Soc.* **2014**, *136*, 64−67.
(19) Zhou, L.; Zhang, C.; McClain, M. J.; Manjavacas, A.; Krauter, C. M.; Tian, S.; Berg, F.; Everitt, H. O.; Carter, E. A.; Nordlander, P. Aluminum nanocrystals as a plasmonic photocatalyst for hydrogen dissociation. *Nano Lett.* **2016**, *16*, 1478−1484.
(20) Huang, Y.-F.; Wu, D.-Y.; Zhu, H.-P.; Zhao, L.-B.; Liu, G.-K.; Ren, B.; Tian, Z.-Q. Surface-enhanced Raman spectroscopic study of p-aminothiophenol. *Phys. Chem. Chem. Phys.* **2012**, *14*, 8485−8497.
(21) Huang, Y.-F.; Zhu, H.-P.; Liu, G.-K.; Wu, D.-Y.; Ren, B.; Tian, Z.-Q. When the signal is not from the original molecule to be detected: chemical transformation of para-aminothiophenol on Ag during the SERS measurement. *J. Am. Chem. Soc.* **2010**, *132*, 9244−9246.
(22) Lou, Z.; Fujitsuka, M.; Majima, T. Pt-Au triangular nanoprisms with strong dipole plasmon resonance for hydrogen generation studied by single-particle spectroscopy. *ACS Nano* **2016**, *10*, 6299−6305.
(23) Wang, F.; Li, C.; Chen, H.; Jiang, R.; Sun, L.-D.; Li, Q.; Wang, J.; Yu, J. C.; Yan, C.-H. Plasmonic harvesting of light energy for Suzuki coupling reactions. *J. Am. Chem. Soc.* **2013**, *135*, 5588−5601.
(24) Wang, F.; Li, C.; Chen, H.; Jiang, R.; Sun, L. D.; Li, Q.; Wang, J.; Yu, J. C.; Yan, C. H. Plasmonic harvesting of light energy for Suzuki coupling reactions. *J. Am. Chem. Soc.* **2013**, *135*, 5588−601.
(25) Sonntag, M. D.; Klingsporn, J. M.; Garibay, L.; Roberts, D.; Dieringer, J. A.; Scheidt, K. A.; Jensen, L.; Schatz, G. C.; Seideman, T.; Van Duyne, R. P. Single Molecule Tip Enhanced Raman Spectroscopy. *J. Phys. Chem. C* **2012**, *116*, 478−483.
(26) Zhang, R.; Zhang, Y.; Dong, Z. C.; Jiang, S.; Zhang, C.; Chen, L. G.; Zhang, L.; Liao, Y.; Aizpurua, J.; Luo, Y.; Yang, J. L.; Hou, J. G. Chemical mapping of a single molecule by plasmon-enhanced Raman scattering. *Nature* **2013**, *498*, 82−6.
(27) Kurouski, D. Advances of tip-enhanced Raman spectroscopy (TERS) in electrochemistry, biochemistry, and surface science. *Vib. Spectrosc.* **2017**, *9*, 3−15.
(28) Bhattarai, A.; Crampton, K. T.; Joly, A. G.; Kovarik, L.; Hess, W. P.; El-Khoury, P. Z. Imaging the Optical Fields of Functionalized Silver Nanowires through Molecular TERS. *J. Phys. Chem. Lett.* **2018**, *9*, 7105−7109.
(29) Bhattarai, A.; Novikova, I. V.; El-Khoury, P. Z. Tip-Enhanced Raman Nanographs of Plasmonic Silver Nanoparticles. *J. Phys. Chem. C* **2019**, *123*, 27765−27769.
(30) Zhong, J. H.; Jin, X.; Meng, L.; Wang, X.; Su, H. S.; Yang, Z. L.; Williams, C. T.; Ren, B. Probing the electronic and catalytic properties of a bimetallic surface with 3 nm resolution. *Nat. Nanotechnol.* **2017**, *12*, 132−136.
(31) Wang, R.; Kurouski, D. Elucidation of Tip-Broadening Effect in Tip-Enhanced Raman Spectroscopy (TERS): A Cause of Artifacts or Potential for 3D TERS. *J. Phys. Chem. C* **2018**, *122*, 24334−24340.
(32) Wang, R.; Li, J.; Rigor, J.; Large, N.; El-Khoury, P.; Rogachev, A. Y.; Kurouski, D. Direct Experimental Evidence of Hot-Carrier-Driven Chemical Processes in Tip-Enhanced Raman Spectroscopy (TERS). *J. Phys. Chem. C* **2020**, *124*, 2238−2244.
(33) Bhattarai, A.; Joly, A. G.; Krayev, A.; El-Khoury, P. Z. Taking the plunge: Nanoscale chemical imaging of functionalized gold triangles in H2O via TERS. *J. Phys. Chem. C* **2019**, *123*, 7376−7380.
(34) Joplin, A.; Hosseini Jebeli, S. A.; Sung, E.; Diemler, N.; Straney, P. J.; Yorulmaz, M.; Chang, W. S.; Millstone, J. E.; Link, S. Correlated Absorption and Scattering Spectroscopy of Individual Platinum-Decorated Gold Nanorods Reveals Strong Excitation Enhancement in the Nonplasmonic Metal. *ACS Nano* **2017**, *11*, 12346−12357.
(35) Chavez, S.; Aslam, U.; Linic, S. Design Principles for Directing Energy and Energetic Charge Flow in Multicomponent Plasmonic Nanostructures. *ACS Energy Lett.* **2018**, *3*, 1590−1596.
(36) Sytwu, K.; Vadai, M.; Dionne, J. A. Bimetallic nanostructures: combining plasmonic and catalytic metals for photocatalysis. *Advances in Physics: X* **2019**, *4*, 394−418.
(37) Wang, J.; Ando, R. A.; Camargo, P. H. Controlling the Selectivity of the Surface Plasmon Resonance Mediated Oxidation of p-Am\inothiophenol on Au Nanoparticles by Charge Transfer from UV-excited TiO2. *Angew. Chem., Int. Ed.* **2015**, *54*, 6909−6912.

https://dx.doi.org/10.1021/acs.jpcc.0c04274
J. Phys. Chem. C XXXX, XXX, XXX−XXX